



Cite this: DOI: 10.1039/c5cs00151j

Phase engineering of transition metal dichalcogenides

Damien Voiry,^a Aditya Mohite^b and Manish Chhowalla^{*a}

Transition metal dichalcogenides (TMDs) represent a family of materials with versatile electronic, optical, and chemical properties. Most TMD bulk crystals are van der Waals solids with strong bonding within the plane but weak interlayer bonding. The individual layers can be readily isolated. Single layer TMDs possess intriguing properties that are ideal for both fundamental and technologically relevant research studies. We review the structure and phases of single and few layered TMDs. We also describe recent progress in phase engineering in TMDs. The ability to tune the chemistry by choosing a unique combination of transition metals and chalcogen atoms along with controlling their properties by phase engineering allows new functionalities to be realized with TMDs.

Received 16th February 2015

DOI: 10.1039/c5cs00151j

www.rsc.org/csr

1. Structure of transition metal dichalcogenides

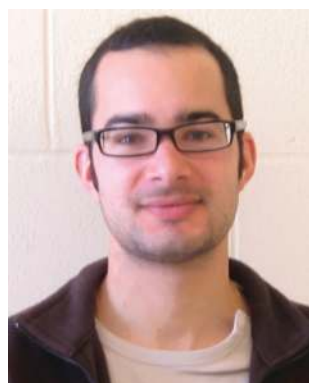
A. 1T, 2H, and 3R polymorphs

Many transition metal dichalcogenides (TMDs) have a layered structure similar to graphites. In TMDs, one unit layer is 3-atoms thick in which the transition metal (M) atom is sandwiched between two chalcogens (X), giving the stoichiometric

MX_2 .¹ The intralayer bonds are covalent, whereas the interlayer bonds between two MX_2 slabs are typically van der Waals bonds. The weak van der Waals bonds allow exfoliation of TMDs down to single layers.² Given the relatively large number of transition metal and chalcogen combinations that can be realized, TMDs with a variety of electronic structures can be realized.^{1,3,4} In contrast to graphene or silicon where the electronic properties are based on hybridization of s and p orbitals, the electronic structure of TMDs depends on the filling of d orbitals of the transition metals. Transition metals in MX_2 compounds have an oxidation state of +4 and the chalcogens have an oxidation state of −2. Thus the number of d orbital electrons varies between 0 and 6 for group 4 to group 10 TMDs, respectively. In addition to

^a Materials Science and Engineering, Rutgers University, 607 Taylor Road, Piscataway, NJ 08854, USA. E-mail: manish1@rci.rutgers.edu

^b Materials Physics and Application Division, Los Alamos National Laboratory, Los Alamos, NM 87545, USA



Damien Voiry

Damien Voiry received his MS degree in materials science from the University of Bordeaux in 2007. He completed his PhD under the supervision of Dr Alain Pénicaud from the University of Bordeaux in 2010. He is currently a postdoctoral researcher in the group of Professor Manish Chhowalla at Rutgers University. His research focuses on two-dimensional materials for electronic and electrochemical applications.



Aditya Mohite

Aditya Mohite obtained his BS and MS in solid state physics from Maharaja Sayajirao University of Baroda in 1999. He received his PhD in Electrical Engineering from the University of Louisville in 2007. After a postdoc at Rice University, he joined the Los Alamos National Laboratory (LANL) in December 2009. Since September 2013, he has been a staff scientist in the department of Materials Science at LANL. His current research aims to understand and control photo-physical processes occurring at the interfaces created using layered 2D materials, organic and inorganic materials for thin film light to energy conversion technologies.

diverse electronic properties that can be achieved by choosing the appropriate combinations of the M and X elements, different phases in single layer TMDs can also be realized. A single layer of TMDs can have a trigonal prismatic phase or an octahedral phase. The trigonal prismatic phase is also referred to as the 2H phase (or 1H in the case of a single layer) and can be described by a hexagonal symmetry (the D_{3h} group) and corresponds to a trigonal prismatic coordination of the metal atoms. This geometry means that in single layers, the sulfur atoms are vertically aligned along the z-axis and the stacking sequence is then AbA where A and b denote chalcogen and metal atoms, respectively (Fig. 1a). The octahedral phase has a tetragonal symmetry (D_{3d}) and corresponds to an octahedral coordination of the metal atoms. In the octahedral phase, conventionally referred to as the 1T phase, one of the sulfur layers is shifted compared to the others resulting in an AbC stacking sequence (Fig. 1b). The filling of the d orbitals of the metal directly influences the atomic structure of the TMD layers. For the 1H phase, the d orbital splits into 3 degenerate states d_{z^2} , $d_{x^2-y^2,xy}$ and $d_{xy,yz}$ with an energy gap of ~ 1 eV between the d_{z^2} and $d_{x^2-y^2,xy}$ orbitals. For the tetragonal symmetry of the 1T phase, the d orbitals of the metal degenerate into $d_{xy,yz,zx}$ (t_{2g}) and $d_{x^2-y^2,z^2}$ (e_g) orbitals. Up to 6 electrons can fill the e_{2g} orbital. Since the p orbitals of chalcogens have been located at much lower energy than the Fermi level, only the filling of the d orbitals determines the nature of phases in MX_2 compounds. Completely filled orbitals give rise to semiconducting behavior while partial filling induces metallic behavior. The type of symmetry of the single layer also strongly depends on the filling of d orbitals. The group 4 (d^0) TMDs and most of the group 6 (d^2) TMDs have trigonal prismatic phases. Group 5 (d^1) TMDs can have both trigonal prismatic or octahedral phases whereas group 7 TMDs have a typically distorted octahedral structure (Fig. 1c). Group 10 TMDs (d^6) have an octahedral phase.

Typically, in single layer TMDs, one of the two possible polytypes is thermodynamically stable. Phase engineering can

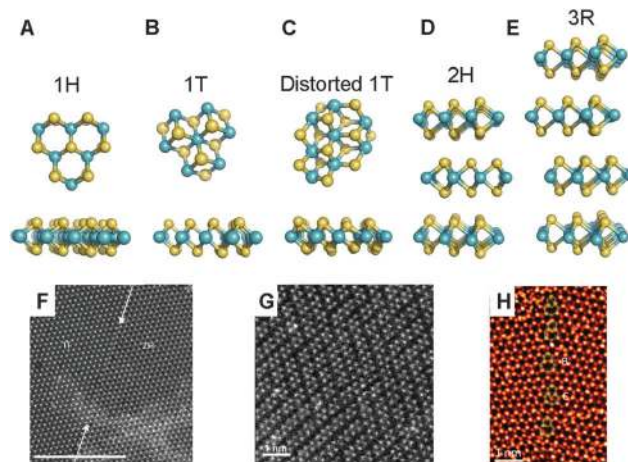


Fig. 1 Different polymorphs or phases of single-layer and stacked single-layer TMDs: (A) 1T phase, (B) ideal ($a \times a$) 1T phase, (C) distorted ($2a \times a$) 1T phase, (D) 2H phase and (E) 3R phase. (F) Scanning transmission electron microscopy (STEM) images of single-layer MoS_2 showing a boundary between the 1T and 2H phases. The arrow indicates the boundary between the phases. Scale bar: 5 nm. Reproduced with permission from ref. 19. Copyright 2014, Nature Publishing Group. (G) STEM image of a lithiated single-layer ReS_2 . After lithiation, the Re atoms form rhombus clusters. Reproduced with permission from ref. 21 with permission from The Royal Society of Chemistry. (H) STEM image of a grain boundary in CVD-grown single-layer MoS_2 . The grain boundary is formed of five- and seven-fold rings (5|7) and dislocations with six- and eight-fold rings (6|8). Reproduced with permission from ref. 53. Copyright 2013, American Chemical Society.

be used to change the polytype as well as the electronic properties of the materials. In addition to the 1T and 1H phases, 2 different ways of stacking the 1H layers can be achieved, imparting hexagonal symmetry (2H phase, symmetry D_{3h}^2) with a stacking sequence of AbA BaB or rhombohedral symmetry (3R, symmetry C_{3v}^2) with the stacking sequence of AbA CaC BcB (Fig. 1d). Stacking in the 1T layer produces the AbC AbC (Fig. 1e) sequence. These heterogeneities in stacking order can not only introduce defects but also lead to interesting new phenomena due to the breaking of symmetry.

B. TMD heterostructures

The phase of single-layer TMDs depends strongly on the d orbital electron density of the transition metal. Tuning the filling of the d orbital enables phase engineering in TMDs. Several examples of phase modification *via* chemical reactions have been reported for group 6 TMDs such as MoS_2 , $MoSe_2$ and WS_2 .^{5–9} Early experiments from Py *et al.* demonstrated the formation of the metallic 1T phase of MoS_2 upon lithium intercalation,¹⁰ which induces reduction of MoS_2 and increases the electron density in the d orbital. As a consequence, group 6 TMDs with the 1T phase are typically negatively charged.¹¹ Similarly the lithiation of TaS_2 induces a phase change from semiconducting 1T phase to metallic 2H phase.¹² Generally, phase transformation in exfoliated single-layer TMDs is not complete and leads to layers containing fractions of both 2H and 1T phases.¹³ Furthermore it has been observed in the case of group 6 TMDs that the 1T phase does not correspond to the



Manish Chhowalla

Manish Chhowalla is a Professor and the Associate Chair of the Materials Science and Engineering Department at Rutgers University. He completed his PhD in Electrical Engineering at the University of Cambridge and he was a Royal Academy of Engineering Postdoctoral Fellow at the same institution. He was the Director of Nanotechnology for the Clean Energy NSF IGERT Program (2009–2014) and the Donald H. Jacobs Chair in

Applied Physics (2009–2011). He is the Editor in Chief of Applied Materials Today. His research interests include the understanding of phase transformations and structural disorder in two-dimensional and other low-dimensional materials.

ideal ($a \times a$) 1T phase of TiS_2 but rather to a distorted 1T phase.^{8,14–16} The 1T phase of group 6 TMDs is unstable. However, the stability can be improved by the formation of a superlattice structure and/or by stabilizing the excess charge on the surface of the reduced TMDs. Four different superstructures have been proposed: a tetramerization ($2a \times 2a$), a trimerization ($\sqrt{3}a \times \sqrt{3}a$), and a zigzag chain ($2a \times a$). The identification of the type of distortion has been debated for a long time. Heising *et al.* have elucidated the distortion of restacked 1T MoS_2 and 1T WS_2 using electron diffraction. Their observations have elucidated that the distorted structure of restacked 1T MoS_2 (WS_2) forms zig-zag chains similar to the structure of WTe_2 with short M–M distances of 0.27 nm and 0.29 nm for W and Mo, respectively.¹⁷ These distances are substantially shorter than typical values of the 2H phase: 0.315 and 0.312 nm for WS_2 and MoS_2 , respectively. These results are in good agreement with STM measurements of Qin *et al.*¹⁵ More recently, HAADF–STEM experiments have enabled direct observation of the atomic structure (Fig. 1f) of the different phases.^{13,18,19} STEM studies of single-layer exfoliated MoS_2/WS_2 after lithium intercalation illustrate the zig-zag chains ($2a \times a$) from the distorted WTe_2 -like 1T phase of MoS_2 and WS_2 together with the ideal 1T TiS_2 -like phase. Other EXAFS and X-ray diffraction experiments on reduced MoS_2 dispersed in solution or intercalated with hydroxide molecules or metal atoms have suggested the existence of a ($2a \times a$) superstructure in the solution. The ($\sqrt{3}a \times \sqrt{3}a$) superstructure has been reported from oxidized $\text{K}_x(\text{H}_2\text{O})_y\text{MoS}_2$ (without the formation of Mo^{6+}) or restacked 1T MoS_2 treated with Br_2 .^{14,17} Similar treatments performed on WS_2 do not induce any observable changes in the superstructure of 1T WS_2 , while the zig-zag distortion is observed in all the cases.¹¹

Interestingly, some TMDs are naturally disordered. 1T WTe_2 (group 6) and 1T ReS_2 (group 5) are good examples of such distorted TMDs with each layer consisting of zig-zag chains of transition metal atoms. Tongay *et al.* have shown that each layer in a bulk crystal of ReS_2 behaves as a monolayer due to the distortion in the 1T phase.²⁰ It has been recently shown that reduction of ReS_2 further increases the distortion and generates Re_4 rhombus clusters (Fig. 1g).²¹

C. Strain in distorted TMDs

The distorted structure of 1T TMDs induces modification of the metal–metal bond distance and thus affects the electronic structure. For example, ReS_2 with 3 electrons in the d orbital is expected to be metallic. However, the strong distortion of the layers forming infinite zig-zag chains of Re atoms opens up an energy gap in the band structure as shown by Kertesz and Hoffmann.²² ReS_2 behaves as a direct band gap semiconductor with a band gap of 1.35 eV and 1.45 eV for the bulk and the monolayer, respectively.²⁰ In addition to the distortion, monolayers of TMDs can be strained. STEM observations of distorted 1T WS_2 have shown an overall isotropic strain of $\sim 3\%$, in agreement with previous X-ray diffraction measurements.²³ DFT simulations of the density of states for distorted 1T phase WS_2 have revealed that strain enhances the density of states

near the Fermi level.²⁴ Recently several groups have predicted that zig-zag chains in 1T phase MoS_2 should open up a small gap of 22–45 meV.^{25,26}

Strain engineering is an intense field of research for the TMD community. DFT calculations have predicted that use of shear or tensile strain²⁶ is another way to tune the properties.^{27–32} Interestingly, biaxial tensile strain leads to a red-shift in the band gap of semiconducting TMDs. Direct to indirect band gap transition is also predicted by stretching of TMDs, thereby making strain engineering particularly interesting for controlling optoelectronic properties. For an isotropic tensile strain of $> 11\%$, 1H MoS_2 and WS_2 become metallic whereas with uniaxial strain, MoS_2 and WS_2 retain their semiconducting properties.^{27,28} Strain has also been shown to improve the catalytic activity of TMDs.^{18,33} Calculations related to strain have also been performed on heterobilayers of MoS_2/MX_2 .³⁴ Experimentally, strain on single-, bi- and tri-layers of MoS_2 has been applied by folding the crystal or bending the substrate.^{35–39} A decrease in the band gap by ~ 45 meV per percent of applied strain has been measured. In addition, direct to indirect transition in the band gap has been observed above $\approx 1\%$ strain (Fig. 2a).³⁵

D. Stacking of TMD layers

The stacking sequence of 1H TMDs can generate the 2H (AB sequence) or 3R (ABC sequence) structures. The ability to grow or exfoliate a variety of single layer TMDs opens up the possibilities of restacking them in desired sequences to achieve novel heterostructures^{34,40–45} (Fig. 2b). Restacked or folded single layer MoS_2 possesses different properties compared to monolayered and bi-layer 2H MoS_2 . The stacking sequence can break the inversion symmetry of bilayer TMDs, allowing an additional pathway for tuning the optical, electronic and spintronic properties of TMDs.⁴⁶ The energy of the indirect transition varies from 1.49 eV to 1.62 eV for twist angles of 0 and 30° (Fig. 2c).⁴⁷ This is attributed to interlayer coupling, which depends on the twist angle between the top and bottom layers of MoS_2 . Restacked bilayer MoS_2 shows strong dependence on interlayer spacing. In the band structure, Mo–d states are found at the K points whereas a mixture of Mo– d_{z^2} and S– p_z are found in the valence band at the Γ point. S– p_z states are dependent on the interlayer stacking, and as a consequence, the energy state at the Γ point is more sensitive to the interlayer coupling than the K point. Additionally the concentration of trions and excitons are also found to depend on the twist angle.⁴⁸ Similar results have been observed from folded MoS_2 although the control over the twist angle is more difficult.

E. Grain boundaries in TMDs

Grain boundaries have been observed in single-layer TMD crystals using dark-field TEM, STEM or second harmonic generation.^{49–52} The grain boundary of MoS_2 displays unique properties, which differ significantly from the properties of an ideal monolayer. STEM observations of TMDs allow direct observation of grain boundaries in monolayered crystals.^{49,50,53} Due to the unique structure of TMDs, various types of dislocations have been observed; such as 5|7 fold rings similar to those reported for

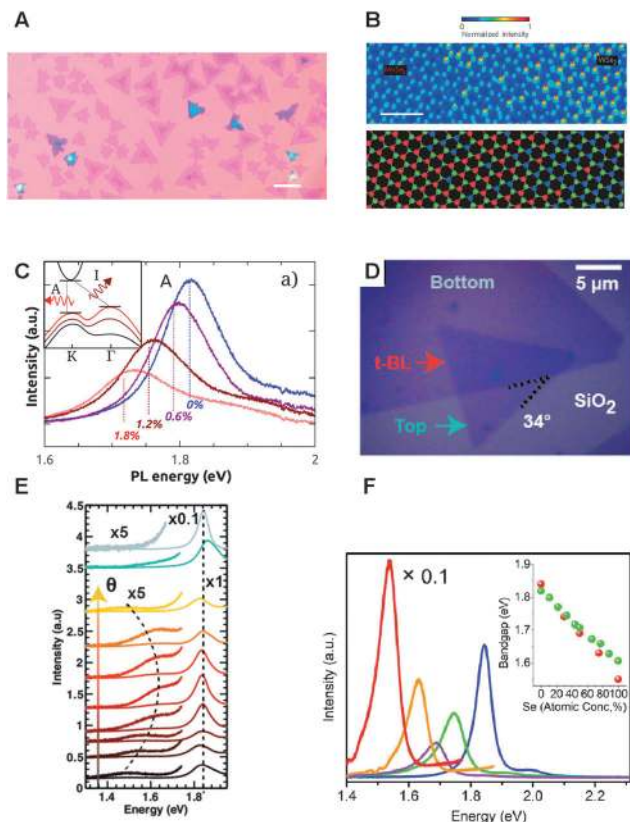


Fig. 2 (A) Optical image of triangular MoSe_2 - WSe_2 heterostructure crystals grown by physical vapor deposition. The core of the triangles consists of MoSe_2 whereas WSe_2 epitaxially grows on the MoSe_2 edges. (B) Top: the color map of the chemical composition of the MoSe_2 - WSe_2 heterostructure observed by STEM. The chemical composition is obtained by the scattered electron intensity. Bottom: restructured structures of the same region. Scale bar: 1 nm. Reproduced with permission from ref. 44. Copyright 2014, Nature Publishing Group. (C) Modification of the photoluminescence spectra of single-layer MoS_2 upon the application of tensile strain. Inset: the band structure of single-layer MoS_2 for 0% (black), -5% (maroon) and -8% (red) of strain. Reproduced with permission from ref. 35. Copyright 2013, American Chemical Society. (D) Optical images of twisted bilayer MoS_2 with an angle of 34° . (E) Photoluminescence (PL) spectra of a bilayer of MoS_2 with a twisting angle from 0° (black) to 60° (yellow). PL spectra from the top and bottom layers are shown in grey and light blue, respectively. Reproduced with permission from ref. 47. Copyright 2014, American Chemical Society. (F) Tuning of the PL response from $\text{MoS}_2(1-x)\text{Se}_{2x}$. Optical response for $x = 0$, $x = 0.3$, $x = 0.5$, $x = 0.75$ and $x = 1$ are shown in blue, green, purple, orange, and red, respectively. The inset shows the comparison between the experimental (red) and the calculated (green) values of the band gap. Reproduced with permission from ref. 56. Copyright 2014, American Chemical Society.

graphene. In addition $4|4$, $4|6$ and $6|8$ fold rings⁵³ have also been observed. Grain boundaries at different angles, $4|4$ and $4|8$ fold rings at 60° versus $6|8$ and $5|7$ fold rings at 18.5° have been found to possess different electronic properties (Fig. 1h). Predictions of local density of states (LDOS) suggest that the 60° grain boundaries with $4|4$ and $4|8$ structures are metallic, which can potentially be used to fabricate novel heterostructures for electronics. Other properties such as magnetism are possible from MoS_2 grain boundaries.⁵⁴ Yakobson and co-workers have reported that $5|7$ dislocations are expected to

be ferromagnetic and the intensity of the magnetism depends on the tilt angle of the dislocations whereas $4|8$ dislocations at tilt angles higher than 48° are favored and are antiferromagnetic.⁵⁴

F. Hybrids with different chalcogens and different transition metals

The synthesis of single layer crystals by chemical vapor deposition has opened up new directions towards realizing alloys of TMDs either by varying the transition metal or chalcogen atoms during growth. For example, selenide doped MoS_2 , $\text{MoS}_2(1-x)\text{Se}_{2x}$, has been obtained *via* a direct synthesis.^{55–57} Typically the doping of MoS_2 with selenide enables modification of the band gap of $\text{MoS}_2(1-x)\text{Se}_{2x}$ from 1.85 eV ($x = 0$) to 1.55 eV ($x = 1$) (Fig. 2d). The PL emission energy varies linearly between the two values with the S concentration, in perfect agreement with theoretical predictions.⁵⁶ STEM observations of $\text{MoS}_2(1-x)\text{Se}_{2x}$ have revealed that the selenium atoms are randomly introduced into the MoS_2 crystal structure.⁵⁶ Alternatively, $\text{MoS}_2(1-x)\text{Se}_{2x}$ can also be obtained by the selenization of already grown 1H MoS_2 crystals. The Se-doping efficiency increases with increasing temperature from 600°C up to 900°C , which allows for tuning of the band gap from 1.86 eV to 1.57 eV.⁵⁸ Alloying two or more transition metals has also been shown to tune the TMD properties.^{59,60} Individual dopants have been observed by electron microscopy modifying the local density of states and potentially the catalytic activity of the materials.^{61,62} Controlled alloying has been more challenging but recent publications have demonstrated the successful synthesis of single layer $\text{Mo}_{(1-x)}\text{W}_x\text{S}_2$ obtained by mechanical exfoliation of the bulk crystal grown by chemical vapor deposition.^{63–66} The presence of both Mo and W atoms in the layers has been confirmed by electron energy loss microscopy. STEM observations have revealed random distribution of Mo and W atoms in the crystal.⁶³ $\text{Mo}_{(1-x)}\text{W}_x\text{S}_2$ have a hexagonal symmetry although some distorted atomic structure has been observed using STEM.⁶⁶ The PL emission of $\text{Mo}_{(1-x)}\text{W}_x\text{S}_2$ was found to vary from 1.82 eV (for $x = 0.2$) to 1.99 eV (for $x = 1$) and the presence of the B exciton peak in the PL spectra suggests that the spin-orbit coupling remains similar to that observed for pristine MoS_2 .

Due to the high melting temperature of transition metal sources (typically metal oxide), the synthesis of TMDs from mixed metals is difficult. The relatively large difference between the melting temperature of precursors can however be used to grow TMD crystals with alternating transition metals. Duan *et al.* have successfully grown MoSe_2 - WSe_2 crystals with lateral heterojunctions using MoSe_2 and WSe_2 powders as precursors (Fig. 2e).⁴⁵ During epitaxial growth, MoSe_2 triangles are first deposited on the substrate. The WSe_2 growth is catalyzed from MoSe_2 edges due to a small lattice mismatch between the materials. Interestingly there is progressive transition from MoSe_2 to WSe_2 (Fig. 2f) and the PL signals from the interface between the two domains consist of a mixture of PL signals from each material. The wide combination of chalcogen and transition metal elements allows for an infinite number of combinations for the synthesis of TMD alloys.

G. Defects and doping in TMDs

Beyond grain boundaries, other types of defects can be observed in TMD crystals. Because of their physical dimensions, 2D materials are very sensitive to the presence of defects in the crystalline structure. The influence of defects has been intensely studied using both DFT calculations and experimental approaches.^{53,67–71} Atomic vacancies are major sources of defects in TMDs. In contrast to graphene, which is made of only one layer of carbon, the alternating X–M–X increase the variety of defects in TMDs. Chalcogen vacancies, metal vacancies or both have been observed experimentally by STEM.⁵³ Chalcogen and metal vacancies are thought to induce profound modification of the electronic structure. For example, in the case of MoS₂, S vacancies are thought to introduce n-type doping whereas Mo vacancies are expected to induce p-type doping. The n-type behavior of MoS₂ is commonly attributed to the lower concentration of S in MoS₂ crystals. Recently McDonnell *et al.* have observed local p- and n-type regions in mechanically exfoliated MoS₂, suggesting that the local stoichiometry might vary significantly from the average macroscopic stoichiometry.⁶⁷ Tongay *et al.* have reported an additional peak at ~1.78 eV in MoS₂ arising from defects in group 6 TMDs.⁶⁸ The new peak is attributed to bound excitons formed by localized excitons at defect sites. S vacancies can coordinate thiol molecules, which could open up new directions for self healing.^{69,70}

Edges of MoS₂ and WS₂ are known to be highly active for hydrogen evolution. TMDs can have metal or chalcogen terminated edges. Van der Zande and coworkers have observed that Mo edges of CVD-grown MoS₂ are usually more sharp and straight than S edges.⁵⁰ Edges of MoS₂ and WS₂ can contain 0%, 50% or 100% sulfur, depending on the synthesis conditions. For example, in the case of industrial catalysts grown on graphitic carbon, MoS₂ nanoclusters have been found to have 50% coverage of Mo edges, whereas large clusters with more than 6 Mo atoms at edges are generally fully sulfur passivated.⁷¹ Recent STEM observations of molybdenum edges of CVD 1H MoS₂ revealed that edges consist of both bare and 50% S covered edges.⁵³

II. Synthesis and characterization of TMDs

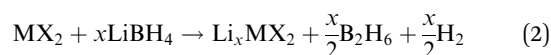
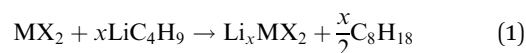
The different synthesis strategies for single layer TMDs can be divided into 3 categories: mechanical exfoliation, liquid exfoliation, and epitaxial growth or chemical vapor deposition. Each of these strategies offers varying quality and yield.

H. Phase engineering *via* alkali metal intercalation

Most experiments on phase engineering of TMDs have used lithium intercalated TMDs. During lithium intercalation, there is an electron transfer from the reducing agent to the structure of TMDs and thus the electron density of the d orbital of the transition metal increases. This induces destabilization of the pristine 2H phase and favors the phase transition to the metallic 1T phase. The first synthesis of single TMDs was reported in the 1980's using chemical exfoliation *via* lithium

intercalation.¹⁰ Original work in Li intercalation in TMDs was motivated by new battery electrode materials.⁷² Pioneering work was performed by Py and Haering in 1983¹⁰ and lithium intercalated MoS₂ is among the most widely studied TMD^{73,74} material. Recent theoretical reports on the intercalation of MoS₂ have shown that the 1T phase becomes more stable than the 2H phase with an excess charge on the exfoliated nanosheets of 0.2–0.4.^{75,76} Moreover DFT calculations have elucidated that the 1T phase consists of a distorted structure rather than the ideal TiS₂-like octahedral phase. Kan *et al.* have predicted that clustering of the metal atoms starts as soon as the octahedral phase is favored.⁷⁶ At 100% intercalation, the crystal structure of MoS₂ corresponds to a distorted octahedral phase with rhombohedral Mo–Mo chains. *In situ* HR-TEM and FFT patterns obtained from Li-intercalated MoS₂ have confirmed the clustering of Mo atoms into a (2a × 2a) superstructure, which can be described as a combination composed of a variety of sublattices, including (a × a), (2a × a), ($\sqrt{3}a \times \sqrt{3}a$), ($\sqrt{3}a \times a$) and (2a × 2a).⁷⁷ After exfoliation, the distortion evolves into a (2a × a) zig-zag WTe₂-type structure as observed by STEM, although the presence of an undistorted TiS₂-like structure has also been identified.^{13,17}

TMDs can be intercalated chemically using lithium reactants, typically *n*-butyllithium diluted in hexane.^{6,78,79} After 48 hours of reaction at room temperature or at reflux, the Li intercalated materials are filtered and washed with hexane in order to remove the excess of butyllithium and other organic byproducts of the reaction (see reaction (1) below). The electron transfer from butyl to the TMD layers implies the insertion of Li⁺ in the van der Waals gap. Alternatively the lithium intercalation can be achieved in the solid state by mixing TMD powder with lithium borohydride (reaction (2) below).^{21,80,81} Powders are mixed together and reaction is performed at 350 °C for 12 hours. The absence of solvents and the fact that the byproduct of the reaction, B₂H₆ and H₂, are gaseous, leave intercalated TMDs clean and free of chemicals used for the phase conversion:



TMDs can also be intercalated electrochemically. Zhang's group has demonstrated the synthesis of intercalated TMDs prepared *via* lithium electrochemical intercalation.⁸² They improved this process further by using the bulk TMDs as cathode materials and the Li metal as the anode.⁸³ Once intercalated, Li_xMX₂ are spontaneously soluble in water. The immersion of Li_xMoS₂ powder in water generates H₂ and potentially H₂S. The mechanism for the exfoliation is not completely elucidated. However, it most likely based on the combination of H₂ bubbling, which separates the nanosheets, and the presence of negative charges on the nanosheets, which stabilizes the exfoliated nanosheets in colloidal solutions.¹¹ It is worth noting that the yield of single layer nanosheets prepared *via* lithium intercalation is high, about 10–20% of the starting bulk powder with a large majority

of the nanosheets in solution as single layers. Although water is the best solvent to achieve complete exfoliation of intercalated TMDs, few studies have been carried out in organic solvents such as formamide and *N*-methylformamide.⁸⁴ The absence of the Moiré pattern in the STEM images confirms the single-layer nature of the exfoliated materials. Eda and co-workers have studied the heterostructure of exfoliated 1T MoS₂ prepared *via* Li-intercalation.¹³ Three phases have been observed: the 1H phase, the non-distorted (TiS₂-like) 1T phase and the distorted (2a × a) 1T phase consisting of zig-zag chains (WTe₂-like structures). The presence of the zig-zag Mo–Mo chains is in good agreement with DFT calculations. The presence of different phases is confirmed by the FFT of the STEM images. A higher amount of the distorted 1T phase has been found in the case of single WS₂ prepared in the same way.²⁴ STEM reveals that existence of the coherent interface between metallic (1T phase) and semiconducting (2H phase) domains.

Other than electron microscopy, identification of the different phases of SL or few-layer TMDs is non-trivial. However, several techniques such as photoluminescence, Raman spectroscopy and X-ray photoelectron electron spectroscopy (XPS) offer fast and relatively precise ways to characterize the heterostructures in TMDs. Changing the phase of TMDs induces changes in the

optoelectronic properties. Emergence or extinction of photoluminescence can easily be detected.⁷⁹ Raman spectroscopy is a powerful tool for estimating the thickness and the phases of the TMD crystals.⁸⁵ Raman spectra of 1T MoS₂ display additional modes: J₁, J₂ and J₃ in addition to the E_{2g}¹ (in-plane) and A_{1g} (out-of-plane modes) of 2H MoS₂ (Fig. 3a).^{7,8} At higher content of the 1T phase, the intensity of the E_{2g}¹ peak decreases. J₁, J₂ and J₃ are attributed to the superlattice structure of the distorted 1T phase.⁷ Recent work by Calandra has validated the vibrational modes of each of the peaks in 1T MoS₂.²⁵ The J₁ mode is the in-plane shearing mode of one side of the zig-zag chain relative to the other. The J₂ mode corresponds to the shifts of the S-atom layers with respect to the Mo atoms whereas the J₃ mode involves the stretching of one side of the zig-zag chain relative to the other with a slightly out-of-plane component. In addition to Raman, XPS can also identify the 1T and 1H (2H) phases of given TMDs. XPS is sensitive to the differences of the Fermi level between the 1T and the 1H (2H) phases as reported by Papageorgopoulos and Jaegerman.⁸⁶ In chemically exfoliated group-6 TMDs, the 1T signal is downshifted by ~0.8 eV relative to the 1H phase. The deconvolution of the high-resolution spectra from the metal and the chalcogen enables the quantitative estimation of the 1T and 2H phases

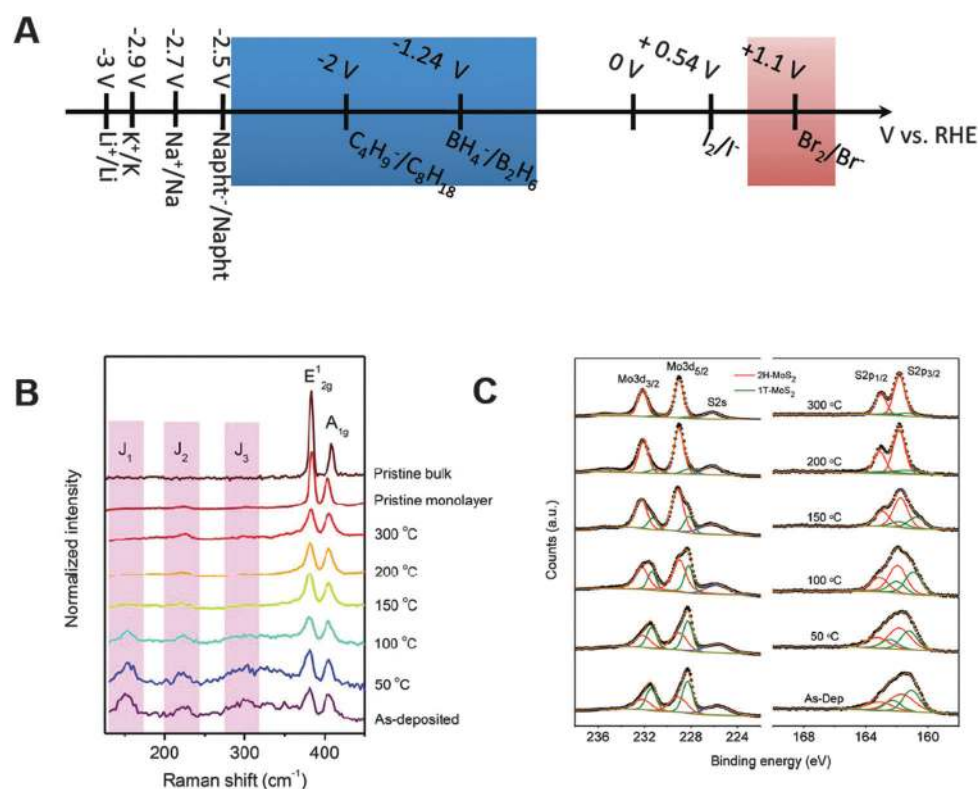


Fig. 3 (A) Potential range of the different redox couples involved in the intercalation and the oxidation of the TMDs. The reduction ($\text{MX}_2/\text{MX}_2^{n-}$) and oxidation (MX_2/MO_x) potential ranges of TMDs are indicated in blue and red, respectively. (B) Evolution of the Raman spectra of chemically exfoliated MoS₂ at increasing annealing temperatures up to 300 °C. As-exfoliated 1T MoS₂ exhibits additional signatures including the J₁, J₂ and J₃ signals. When increasing the annealing temperature, the signals from the 1T phase progressively decrease. (C) High-resolution X-ray photoelectron spectra from the Mo3d and S2p regions of chemically exfoliated MoS₂. Each spectrum can be decomposed with 2 components from the 1T and the 2H phases. The signals from the 1T phase are found to be downshifted ~0.8–0.9 eV relative to the 2H signals. Reproduced with permission from ref. 79. Copyright 2011, American Chemical Society.

(Fig. 3b).^{24,79} However the type of 1T phase, ideal undistorted or distorted, cannot be elucidated by XPS and so far only STEM can unambiguously identify the atomic structure of the 1T phase.

Alternate routes based on intercalation have also been reported using other alkali metals.^{84,87} Systematic studies of exfoliation of TMDs with different counter-ions have been carried out by Zheng and co-workers using naphthalenide as the reducing agent instead of butyl in the case of butyllithium.⁸⁷ The crystals of TMDs were first pre-exfoliated using hydrazine before intercalation with different alkali metals. This route produces large single nanosheets with lateral dimensions $> 5 \mu\text{m}$. The highest quality of exfoliated nanosheets was obtained using Na intercalated TMDs. Although the phase transition has not been investigated, similar phase transition upon filling the d orbitals of the transition metals is expected during the reaction with naphthalenide.

I. Alternative strategies for phase engineering

The emergence of phase engineered TMDs has driven efforts to develop alternative synthetic routes. Lin and coworkers reported the synthesis of undistorted 1T MoS_2 by using electron beam.⁶² Using e-beam irradiation, the 2H phase converts into a new phase (denoted as α) forming two atomic stripes with an angle of 60° (Fig. 4a). Each strip of atoms consists of three to four constricted MoS_2 zig-zag chains with a reduced Mo–Mo distance measured using STEM. At the intersection of the two stripes, the atoms are so packed that it triggers the formation of the 1T phase to release the strain. As the e-beam irradiation of the MoS_2 layer continues, the 1T phase domain progressively grows forming a triangular shape. The boundary of the 1T triangle with the 2 phases shows two new atomic arrangements denoted as β and γ (Fig. 4a). Thus electron beam can be used to very precisely pattern TMDs with alternating 1T and 2H phases, allowing for the creation of well-defined geometries with abrupt metal–semiconductor interfaces. Alternatively, phase transitions have also been observed from the electron transfer of plasmonic hot electrons to CVD grown MoS_2 .⁸⁸ Gold nanoparticles were used as plasmonic nanoparticles and deposited on the surface of TMDs (typically MoS_2) with a loading density of $10^4 \mu\text{m}^{-2}$. Under light exposure, the hot electrons are transferred to MoS_2 crystals. The 1T phase formation was confirmed by PL measurements and Raman spectroscopy.

Tensile or compressive strain can be also be used to tune the properties of TMDs. Several contributions have demonstrated that it is possible to modify the photoluminescence signals of group-6 TMDs *via* strain engineering. A recent report from Duerloo and coworkers has introduced the possibility of thermodynamically inducing phase transition through mechanical deformation of the group-6 TMDs.⁸⁹ According to their calculations, the conversion from the 1H phase to the distorted WTe_2 -like 1T phase can be achieved by applying strain on the TMD structure. The percent strain required to achieve the phase transition depends on the specific TMD used, but is still below the threshold for breaking the TMD layers. The best candidate for such mechanical switching of the structural phase is MoTe_2 with a minimal tensile strain of 0.3–3% at room temperature.

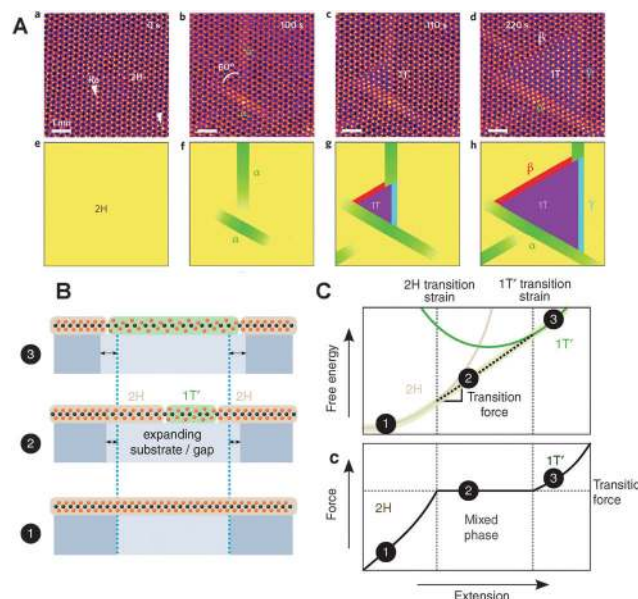


Fig. 4 (A) 2H to 1T transformation of a single-layer of MoS_2 under electron-beam irradiation. After 100s, a new phase (denoted as α) forms on the MoS_2 basal plane forming two stripes with an angle of 60° . Rapidly the 2H phase between the two stripes convert into the 1T phase. As time increases, the 1T phase domains grow and two new types of boundaries, denoted as β and γ , appear. Reproduced with permission from ref. 62. Copyright 2014, Nature Publishing Group. (B) 2H to 1T phase transformation of single-layer TMDs when applying uniaxial strain. The region quasi freely suspended or on a low-friction substrate (middle) is converted. (C) Evolution of the free energy and the force when applying uniaxial deformation. In the beginning (step 1) the 2H phase deforms elastically without phase transition. In step 2, the lowest free-energy path is a common tangent between the 2H and distorted 1T ($1T'$) energy surfaces and co-existence of both phases is predicted. This region corresponds to a plateau in the applied force. Increasing further the extension leads to the formation of 100% distorted 1T phase. Reproduced with permission from ref. 89. Copyright 2014, Nature Publishing Group.

These predictions allow imagining that phase transition could be achieved by depositing the crystals on a bended flexible substrate or by using atomic force microscopy (Fig. 4b).

Several groups have reported the chemical synthesis of TMDs *via* colloidal synthesis^{90–92} or hydrothermal reaction.⁹³ This method enables the synthesis of a large quantity of few-layered thin TMDs *via* various types of precursors. Hybrid materials such as TMD/reduced graphene oxide (rGO) can be synthesized in this way.^{94,95} By changing the synthesis conditions different concentrations of defects (vacancies and oxygen atoms) can be incorporated into the TMD atomic structure, which has been found to improve the catalytic activity towards the hydrogen evolution reaction.^{96,97} Colloidal synthesis could also be used for the synthesis of alloy-based TMDs with various transition metals or chalcogens. The most thermodynamically stable phase is typically obtained *via* colloidal synthesis, which limits the possibility of tuning the crystal phases. Recent work from Ozin's group has demonstrated the possibility of controlling the synthesis of the enriched 1T phase of WS_2 .⁹⁸ The modification of the reaction conditions in order to slow the reaction rate induces the preferential growth of the single-layer 1T phase. The 1T

nanosheets are negatively charged, which prevents aggregation. The nanosheets present a distorted structure similar to the structure of chemically exfoliated 1T WS₂ prepared *via* lithium intercalation.¹⁸ Further improvements of the colloidal synthesis of TMD nanosheets is expected to open up new directions towards the growth of highly crystalline 1T and 1H phases.

The recent progress in chemical vapor deposition (CVD) or the epitaxial growth opens up new avenues for realizing phase engineering in TMDs while maintaining high degree of crystallinity. The most common method to grow TMDs by CVD is to use metal oxide and the chalcogen powders as the source of transition metals and chalcogen, respectively.^{49,50} Alternatively, few examples of liquid precursors such as thiomolybdate can be found in the literature.⁹⁹ As discussed earlier in this review, few examples of alloys of CVD-grown TMD have been reported. Single layers of mixed TMDs with lateral or vertical heterojunctions have been prepared *via* epitaxial growth.^{43–45} Chemical vapor deposition favors the growth of the most stable phase and thus the possibility of obtaining different phases is limited. Chemical vapor deposition based growth of TMDs with different phases that are usually not stable such as the 1T phase for group 6 would open up new possibilities to the field. Such growth has not been reported to date. However, Wypych *et al.* reported the growth of pure and highly crystalline bulk 1T MoS₂ by the sulfurization of potassium molybdate.¹⁰⁰ Potassium molybdate K₂MoO₄ was first sulfurized at $T < 500$ °C for 24 hours followed by reduction at 850 °C for 72 hours under a flow of H₂/N₂. This yields bulk KMoS₂ crystals with highly crystalline 1T phase of MoS₂ as confirmed using XRD diffraction. The presence of potassium counterions in the materials stabilizes the 1T phase and favors its formation. The crystal can then be washed with water to remove the potassium cations.

J. Stability of the 1T phase

Engineering the phases of TMDs has been considered illusive due to the fact that TMDs have usually one phase that is thermodynamically stable. Yet the most stable 2H (1T) phase can be converted into the 1T (2H) phase. Up to now, most of the efforts have been focused on group 6 TMDs. Various characterization techniques including STEM, TEM, electron diffraction, Raman and XPS spectroscopy have confirmed the stability of the 1T phase under ambient conditions in the absence of lithium^{13,24} in agreement with theoretical predictions.^{26,75} The origin of the stability of the 1T phase is probably due to structural distortion and the presence of counterions. The presence of dopant impurities such as Au or Re may also contribute to the stabilization.⁶² Heising and Kanatzidis demonstrated that exfoliated 1T nanosheets are negatively charged with a charge excess of ~ 0.3 charges per MX₂.¹¹ The quantity of charges is however reduced compared to the initial stoichiometry of intercalated materials, Li _{~ 1} MX₂. Some of the charges react with water forming hydrogen (H₂) during the exfoliation process. The reduction of the charges could explain why the metal atoms form zig-zag patterns in the case of exfoliated 1T MoS₂/WS₂, and calculations have predicted that with excess charges corresponding to d^{2.0–2.5}, zig-zag chains of Mo atoms are more favored.¹⁰¹ The charges carried by 1T

MoS₂/WS₂ can be reduced by using a mild oxidizing agent such as Br₂ or I₂ as confirmed by zeta potential measurements.⁸¹ Even after the quenching of the charges, the distorted ($2a \times a$) 1T phase is present according to Raman spectroscopy and STEM.⁸¹ Heising and Kanatzidis have also observed the distorted 1T phase with ($2a \times a$) and ($\sqrt{3}a \times \sqrt{3}a$) lattices with WS₂ and MoS₂, respectively, treated with Br₂.¹¹ DSC measurements of 1T MoS₂ and WS₂ have shown that the 1T to 1H transition occurs at significantly higher temperatures in the case of 1T WS₂ (~ 195 °C) compared to 1T MoS₂ (~ 95 °C). Interestingly the oxidation of 1T WS₂ and 1T MoS₂ with Br₂ induces a decrease in the transition temperature at ~ 145 °C and ~ 90 °C respectively, suggesting the role of the charges (and counterions) on the stability of the phase engineered TMDs.^{11,80} This relatively high transition temperature indicates that although the 2H phase is more stable, there is an energy barrier as high as ~ 0.87 eV for the 1T to 2H transformation²⁴ in good agreement with DFT calculations: 0.95 eV.⁸⁰

III. Conclusions and perspectives

We have highlighted key progress in phase engineering of single layered transition metal dichalcogenides. Phase engineering in TMDs offers opportunities for doing both fundamental and technologically relevant research. Researchers are therefore actively involved in elucidating new methods for phase engineering in TMDs. Currently, phase engineering has been achieved by alkali metal intercalation, electron beam irradiation and strain engineering. Of these, lithium intercalation has a long history and thus has been widely studied. The recent results on the fabrication of lateral heterostructures of metallic and semiconducting phases have led to the realization of novel electronic devices with very low contact resistances. Phase engineering has also benefitted in making better catalysts. Thus there is a tremendous amount of interest in this topic.

Although TMDs can exist in a variety of different phases, the main trick is to engineer those phases in a desired manner in the same material. That is, to induce the metallic 1T phase in a semiconducting 1H TMD and *vice versa*. Presently it is not possible to realize single layer 1T phase TMD compounds due to stability issues. This has hampered progress in fundamental research because the 1T phase in two-dimensional systems could hold novel condensed matter phenomena. Our approach is to induce the 1T phase in stable 1H phase materials. The ability of fully converting a 1H phase TMD into a 1T phase TMD will allow investigations of novel properties of the metallic phase.

References

- 1 J. A. Wilson and A. D. Yoffe, *Adv. Phys.*, 1969, **18**, 193–335.
- 2 K. S. Novoselov, D. Jiang, F. Schedin, T. J. Booth, V. V. Khotkevich, S. V. Morozov and A. K. Geim, *Proc. Natl. Acad. Sci. U. S. A.*, 2005, **102**, 10451–10453.
- 3 L. F. Mattheiss, *Phys. Rev. B: Solid State*, 1973, **8**, 3719–3740.

- 4 Q. H. Wang, K. Kalantar-Zadeh, A. Kis, J. N. Coleman and M. S. Strano, *Nat. Nanotechnol.*, 2012, **7**, 699–712.
- 5 P. Joensen, R. F. Frindt and S. R. Morrison, *Mater. Res. Bull.*, 1986, **21**, 457–461.
- 6 B. K. Miremadi and S. R. Morrison, *J. Appl. Phys.*, 1988, **63**, 4970–4974.
- 7 S. Jiménez Sandoval, D. Yang, R. F. Frindt and J. C. Irwin, *Phys. Rev. B: Condens. Matter Mater. Phys.*, 1991, **44**, 3955–3962.
- 8 D. Yang, S. J. Sandoval, W. M. Divigalpitiya, J. C. Irwin and R. F. Frindt, *Phys. Rev. B: Condens. Matter Mater. Phys.*, 1991, **43**, 12053–12056.
- 9 R. A. Gordon, D. Yang, E. D. Crozier, D. T. Jiang and R. F. Frindt, *Phys. Rev. B: Condens. Matter Mater. Phys.*, 2002, **65**, 125407.
- 10 M. A. Py and R. R. Haering, *Can. J. Phys.*, 1983, **61**, 76–84.
- 11 J. Heising and M. G. Kanatzidis, *J. Am. Chem. Soc.*, 1999, **121**, 11720–11732.
- 12 P. Ganal, W. Olberding, T. Butz and G. Ouvrard, *Solid State Ionics*, 1993, **59**, 313–319.
- 13 G. Eda, T. Fujita, H. Yamaguchi, D. Voiry, M. Chen and M. Chhowalla, *ACS Nano*, 2012, **6**, 7311–7317.
- 14 F. Wypych, T. Weber and R. Prins, *Chem. Mater.*, 1998, **10**, 723–727.
- 15 X. R. Qin, D. Yang, R. F. Frindt and J. C. Irwin, *Phys. Rev. B: Condens. Matter Mater. Phys.*, 1991, **44**, 3490–3493.
- 16 X. R. Qin, D. Yang, R. F. Frindt and J. C. Irwin, *Ultramicroscopy*, 1992, **42–44**(Part 1), 630–636.
- 17 J. Heising and M. G. Kanatzidis, *J. Am. Chem. Soc.*, 1999, **121**, 638–643.
- 18 D. Voiry, H. Yamaguchi, J. Li, R. Silva, D. C. B. Alves, T. Fujita, M. Chen, T. Asefa, V. B. Shenoy, G. Eda and M. Chhowalla, *Nat. Mater.*, 2013, **12**, 850–855.
- 19 R. Kappera, D. Voiry, S. E. Yalcin, B. Branch, G. Gupta, A. D. Mohite and M. Chhowalla, *Nat. Mater.*, 2014, **13**, 1128–1134.
- 20 S. Tongay, H. Sahin, C. Ko, A. Luce, W. Fan, K. Liu, J. Zhou, Y.-S. Huang, C.-H. Ho, J. Yan, D. F. Ogletree, S. Aloni, J. Ji, S. Li, J. Li, F. M. Peeters and J. Wu, *Nat. Commun.*, 2014, **5**, 3252.
- 21 T. Fujita, Y. Ito, Y. Tan, H. Yamaguchi, D. Hoko, A. Hirata, D. A. Voiry, M. Chhowalla and M. Chen, *Nanoscale*, 2014, **6**, 12458–12462.
- 22 M. Kertesz and R. Hoffmann, *J. Am. Chem. Soc.*, 1984, **106**, 3453–3460.
- 23 D. Yang and R. F. Frindt, *J. Phys. Chem. Solids*, 1996, **57**, 1113–1116.
- 24 D. Voiry, H. Yamaguchi, J. Li, R. Silva, D. C. B. Alves, T. Fujita, M. Chen, T. Asefa, V. B. Shenoy, G. Eda and M. Chhowalla, *Nat. Mater.*, 2013, **12**, 850–855.
- 25 M. Calandra, *Phys. Rev. B: Condens. Matter Mater. Phys.*, 2013, **88**, 245428.
- 26 M. Kan, J. Y. Wang, X. W. Li, S. H. Zhang, Y. W. Li, Y. Kawazoe, Q. Sun and P. Jena, *J. Phys. Chem. C*, 2014, **118**, 1515–1522.
- 27 P. Johari and V. B. Shenoy, *ACS Nano*, 2012, **6**, 5449–5456.
- 28 M. Ghorbani-Asl, S. Borini, A. Kuc and T. Heine, *Phys. Rev. B: Condens. Matter Mater. Phys.*, 2013, **87**, 235434.
- 29 L. Kou, A. Du, C. Chen and T. Frauenheim, *Nanoscale*, 2014, **6**, 5156–5161.
- 30 P. Lu, X. Wu, W. Guo and X. C. Zeng, *Phys. Chem. Chem. Phys.*, 2012, **14**, 13035–13040.
- 31 H. Peelaers and C. G. Van de Walle, *Phys. Rev. B: Condens. Matter Mater. Phys.*, 2012, **86**, 241401.
- 32 L. Yang, X. Cui, J. Zhang, K. Wang, M. Shen, S. Zeng, S. A. Dayeh, L. Feng and B. Xiang, *Sci. Rep.*, 2014, **4**, 5649.
- 33 J. H. Lee, W. S. Jang, S. W. Han and H. K. Baik, *Langmuir*, 2014, **30**, 9866–9873.
- 34 N. Lu, H. Guo, L. Li, J. Dai, L. Wang, W.-N. Mei, X. Wu and X. C. Zeng, *Nanoscale*, 2014, **6**, 2879–2886.
- 35 H. J. Conley, B. Wang, J. I. Ziegler, R. F. Haglund, S. T. Pantelides and K. I. Bolotin, *Nano Lett.*, 2013, **13**, 3626–3630.
- 36 K. He, C. Poole, K. F. Mak and J. Shan, *Nano Lett.*, 2013, **13**, 2931–2936.
- 37 C. R. Zhu, G. Wang, B. L. Liu, X. Marie, X. F. Qiao, X. Zhang, X. X. Wu, H. Fan, P. H. Tan, T. Amand and B. Urbaszek, *Phys. Rev. B: Condens. Matter Mater. Phys.*, 2013, **88**, 121301.
- 38 A. Castellanos-Gomez, R. Roldán, E. Cappelluti, M. Buscema, F. Guinea, H. S. J. van der Zant and G. A. Steele, *Nano Lett.*, 2013, **13**, 5361–5366.
- 39 Y. Y. Hui, X. Liu, W. Jie, N. Y. Chan, J. Hao, Y.-T. Hsu, L.-J. Li, W. Guo and S. P. Lau, *ACS Nano*, 2013, **7**, 7126–7131.
- 40 L. Kou, T. Frauenheim and C. Chen, *J. Phys. Chem. Lett.*, 2013, **4**, 1730–1736.
- 41 H.-P. Komsa and A. V. Krashenninnikov, *Phys. Rev. B: Condens. Matter Mater. Phys.*, 2013, **88**, 085318.
- 42 G. Gao, W. Gao, E. Cannuccia, J. Taha-Tijerina, L. Balicas, A. Mathkar, T. N. Narayanan, Z. Liu, B. K. Gupta, J. Peng, Y. Yin, A. Rubio and P. M. Ajayan, *Nano Lett.*, 2012, **12**, 3518–3525.
- 43 Y. Gong, J. Lin, X. Wang, G. Shi, S. Lei, Z. Lin, X. Zou, G. Ye, R. Vajtai, B. I. Yakobson, H. Terrones, M. Terrones, B. K. Tay, J. Lou, S. T. Pantelides, Z. Liu, W. Zhou and P. M. Ajayan, *Nat. Mater.*, 2014, **13**, 1135–1142.
- 44 C. Huang, S. Wu, A. M. Sanchez, J. J. P. Peters, R. Beanland, J. S. Ross, P. Rivera, W. Yao, D. H. Cobden and X. Xu, *Nat. Mater.*, 2014, **13**, 1096–1101.
- 45 X. Duan, C. Wang, J. C. Shaw, R. Cheng, Y. Chen, H. Li, X. Wu, Y. Tang, Q. Zhang, A. Pan, J. Jiang, R. Yu, Y. Huang and X. Duan, *Nat. Nanotechnol.*, 2014, **9**, 1024–1030.
- 46 T. Jiang, H. Liu, D. Huang, S. Zhang, Y. Li, X. Gong, Y.-R. Shen, W.-T. Liu and S. Wu, *Nat. Nanotechnol.*, 2014, **9**, 825–829.
- 47 A. M. van der Zande, J. Kunstmann, A. Chernikov, D. A. Chenet, Y. You, X. Zhang, P. Y. Huang, T. C. Berkelbach, L. Wang, F. Zhang, M. S. Hybertsen, D. A. Muller, D. R. Reichman, T. F. Heinz and J. C. Hone, *Nano Lett.*, 2014, **14**, 3869–3875.
- 48 S. Huang, X. Ling, L. Liang, J. Kong, H. Terrones, V. Meunier and M. S. Dresselhaus, *Nano Lett.*, 2014, **14**, 5500–5508.

- 49 S. Najmaei, Z. Liu, W. Zhou, X. Zou, G. Shi, S. Lei, B. I. Yakobson, J.-C. Idrobo, P. M. Ajayan and J. Lou, *Nat. Mater.*, 2013, **12**, 754–759.
- 50 A. M. van der Zande, P. Y. Huang, D. A. Chenet, T. C. Berkelbach, Y. You, G.-H. Lee, T. F. Heinz, D. R. Reichman, D. A. Muller and J. C. Hone, *Nat. Mater.*, 2013, **12**, 554–561.
- 51 X. Yin, Z. Ye, D. A. Chenet, Y. Ye, K. O'Brien, J. C. Hone and X. Zhang, *Science*, 2014, **344**, 488–490.
- 52 Y. Zhang, Y. Zhang, Q. Ji, J. Ju, H. Yuan, J. Shi, T. Gao, D. Ma, M. Liu, Y. Chen, X. Song, H. Y. Hwang, Y. Cui and Z. Liu, *ACS Nano*, 2013, **7**, 8963–8971.
- 53 W. Zhou, X. Zou, S. Najmaei, Z. Liu, Y. Shi, J. Kong, J. Lou, P. M. Ajayan, B. I. Yakobson and J.-C. Idrobo, *Nano Lett.*, 2013, **13**, 2615–2622.
- 54 Z. Zhang, X. Zou, V. H. Crespi and B. I. Yakobson, *ACS Nano*, 2013, **7**, 10475–10481.
- 55 H. Li, X. Duan, X. Wu, X. Zhuang, H. Zhou, Q. Zhang, X. Zhu, W. Hu, P. Ren, P. Guo, L. Ma, X. Fan, X. Wang, J. Xu, A. Pan and X. Duan, *J. Am. Chem. Soc.*, 2014, **136**, 3756–3759.
- 56 Y. Gong, Z. Liu, A. R. Lupini, G. Shi, J. Lin, S. Najmaei, Z. Lin, A. L. Elías, A. Berkdemir, G. You, H. Terrones, M. Terrones, R. Vajtai, S. T. Pantelides, S. J. Pennycook, J. Lou, W. Zhou and P. M. Ajayan, *Nano Lett.*, 2014, **14**, 442–449.
- 57 J. Mann, Q. Ma, P. M. Odenthal, M. Isarraraz, D. Le, E. Preciado, D. Barroso, K. Yamaguchi, G. von Son Palacio, A. Nguyen, T. Tran, M. Wurch, A. Nguyen, V. Klee, S. Bobek, D. Sun, T. F. Heinz, T. S. Rahman, R. Kawakami and L. Bartels, *Adv. Mater.*, 2014, **26**, 1399–1404.
- 58 S.-H. Su, Y.-T. Hsu, Y.-H. Chang, M.-H. Chiu, C.-L. Hsu, W.-T. Hsu, W.-H. Chang, J.-H. He and L.-J. Li, *Small*, 2014, **10**, 2589–2594.
- 59 A. Kutana, E. S. Penev and B. I. Yakobson, *Nanoscale*, 2014, **6**, 5820–5825.
- 60 J. Xi, T. Zhao, D. Wang and Z. Shuai, *J. Phys. Chem. Lett.*, 2014, **5**, 285–291.
- 61 Y.-C. Lin, D. O. Dumcenco, H.-P. Komsa, Y. Niimi, A. V. Krashenninnikov, Y.-S. Huang and K. Suenaga, *Adv. Mater.*, 2014, **26**, 2857–2861.
- 62 Y.-C. Lin, D. O. Dumcenco, Y.-S. Huang and K. Suenaga, *Nat. Nanotechnol.*, 2014, **9**, 391–396.
- 63 Y. Chen, J. Xi, D. O. Dumcenco, Z. Liu, K. Suenaga, D. Wang, Z. Shuai, Y.-S. Huang and L. Xie, *ACS Nano*, 2013, **7**, 4610–4616.
- 64 Q. Feng, Y. Zhu, J. Hong, M. Zhang, W. Duan, N. Mao, J. Wu, H. Xu, F. Dong, F. Lin, C. Jin, C. Wang, J. Zhang and L. Xie, *Adv. Mater.*, 2014, **26**, 2648–2653.
- 65 S. Tongay, D. S. Narang, J. Kang, W. Fan, C. Ko, A. V. Luce, K. X. Wang, J. Suh, K. D. Patel, V. M. Pathak, J. Li and J. Wu, *Appl. Phys. Lett.*, 2014, **104**, 012101.
- 66 D. O. Dumcenco, H. Kobayashi, Z. Liu, Y.-S. Huang and K. Suenaga, *Nat. Commun.*, 2013, **4**, 1351.
- 67 S. McDonnell, R. Addou, C. Buie, R. M. Wallace and C. L. Hinkle, *ACS Nano*, 2014, **8**, 2880–2888.
- 68 S. Tongay, J. Suh, C. Ataca, W. Fan, A. Luce, J. S. Kang, J. Liu, C. Ko, R. Raghunathanan, J. Zhou, F. Ogletree, J. Li, J. C. Grossman and J. Wu, *Sci. Rep.*, 2013, **3**, 2657.
- 69 M. Makarova, Y. Okawa and M. Aono, *J. Phys. Chem. C*, 2012, **116**, 22411–22416.
- 70 S. S. Chou, M. De, J. Kim, S. Byun, C. Dykstra, J. Yu, J. Huang and V. P. Dravid, *J. Am. Chem. Soc.*, 2013, **135**, 4584–4587.
- 71 L. P. Hansen, Q. M. Ramasse, C. Kisielowski, M. Brorson, E. Johnson, H. Topsøe and S. Helveg, *Angew. Chem., Int. Ed.*, 2011, **50**, 10153–10156.
- 72 I. Samaras, S. I. Saikh, C. Julien and M. Balkanski, *Mater. Sci. Eng., B*, 1989, **3**, 209–214.
- 73 M. B. Dines, *Mater. Res. Bull.*, 1975, **10**, 287–291.
- 74 M. S. Whittingham and F. R. Gamble Jr., *Mater. Res. Bull.*, 1975, **10**, 363–371.
- 75 A. N. Enyashin and G. Seifert, *Comput. Theor. Chem.*, 2012, **999**, 13–20.
- 76 M. Kan, J. Y. Wang, X. W. Li, S. H. Zhang, Y. W. Li, Y. Kawazoe, Q. Sun and P. Jena, *J. Phys. Chem. C*, 2014, **118**, 1515–1522.
- 77 L. Wang, Z. Xu, W. Wang and X. Bai, *J. Am. Chem. Soc.*, 2014, **136**, 6693–6697.
- 78 P. Joensen, R. F. Frindt and S. R. Morrison, *Mater. Res. Bull.*, 1986, **21**, 457–461.
- 79 G. Eda, H. Yamaguchi, D. Voiry, T. Fujita, M. Chen and M. Chhowalla, *Nano Lett.*, 2011, **11**, 5111–5116.
- 80 H.-L. Tsai, J. Heising, J. L. Schindler, C. R. Kannewurf and M. G. Kanatzidis, *Chem. Mater.*, 1997, **9**, 879–882.
- 81 D. Voiry, M. Salehi, R. Silva, T. Fujita, M. Chen, T. Asefa, V. B. Shenoy, G. Eda and M. Chhowalla, *Nano Lett.*, 2013, **13**, 6222–6227.
- 82 Z. Zeng, Z. Yin, X. Huang, H. Li, Q. He, G. Lu, F. Boey and H. Zhang, *Angew. Chem., Int. Ed.*, 2011, **50**, 11093–11097.
- 83 Z. Zeng, T. Sun, J. Zhu, X. Huang, Z. Yin, G. Lu, Z. Fan, Q. Yan, H. H. Hng and H. Zhang, *Angew. Chem., Int. Ed.*, 2012, **51**, 9052–9056.
- 84 A. Lerf and R. Schoellhorn, *Inorg. Chem.*, 1977, **16**, 2950–2956.
- 85 C. Lee, H. Yan, L. E. Brus, T. F. Heinz, J. Hone and S. Ryu, *ACS Nano*, 2010, **4**, 2695–2700.
- 86 C. A. Papageorgopoulos and W. Jaegermann, *Surf. Sci.*, 1995, **338**, 83–93.
- 87 J. Zheng, H. Zhang, S. Dong, Y. Liu, C. Tai Nai, H. Suk Shin, H. Young Jeong, B. Liu and K. Ping Loh, *Nat. Commun.*, 2014, **5**, 2995.
- 88 Y. Kang, S. Najmaei, Z. Liu, Y. Bao, Y. Wang, X. Zhu, N. J. Halas, P. Nordlander, P. M. Ajayan, J. Lou and Z. Fang, *Adv. Mater.*, 2014, **26**, 6467–6471.
- 89 K.-A. N. Duerloo, Y. Li and E. J. Reed, *Nat. Commun.*, 2014, **5**, 4214.
- 90 X. Zhou, J. Jiang, T. Ding, J. Zhang, B. Pan, J. Zuo and Q. Yang, *Nanoscale*, 2014, **6**, 11046–11051.
- 91 D. Yoo, M. Kim, S. Jeong, J. Han and J. Cheon, *J. Am. Chem. Soc.*, 2014, **136**, 14670–14673.
- 92 P. Miró, J. H. Han, J. Cheon and T. Heine, *Angew. Chem., Int. Ed.*, 2014, **46**, 12624–12628.
- 93 X. Chen and R. Fan, *Chem. Mater.*, 2001, **13**, 802–805.

- 94 Y. Li, H. Wang, L. Xie, Y. Liang, G. Hong and H. Dai, *J. Am. Chem. Soc.*, 2011, **133**, 7296–7299.
- 95 J. Yang, D. Voiry, A. Y. Kim, M. Chhowalla and H. S. Shin, *Angew. Chem., Int. Ed.*, 2013, **52**, 13751–13754.
- 96 J. Xie, H. Zhang, S. Li, R. Wang, X. Sun, M. Zhou, J. Zhou, X. W. (David) Lou and Y. Xie, *Adv. Mater.*, 2013, **25**, 5807–5813.
- 97 J. Xie, J. Zhang, S. Li, F. Grote, X. Zhang, H. Zhang, R. Wang, Y. Lei, B. Pan and Y. Xie, *J. Am. Chem. Soc.*, 2013, **135**, 17881–17888.
- 98 B. Mahler, V. Hoepfner, K. Liao and G. A. Ozin, *J. Am. Chem. Soc.*, 2014, **136**, 14121–14127.
- 99 K.-K. Liu, W. Zhang, Y.-H. Lee, Y.-C. Lin, M.-T. Chang, C.-Y. Su, C.-S. Chang, H. Li, Y. Shi, H. Zhang, C.-S. Lai and L.-J. Li, *Nano Lett.*, 2012, **12**, 1538–1544.
- 100 F. Wypych and R. Schöllhorn, *J. Chem. Soc., Chem. Commun.*, 1992, 1386–1388.
- 101 J. K. Burdett and T. Hughbanks, *Inorg. Chem.*, 1985, **24**, 1741–1750.